

## A comprehensive simulation model of the performance of photochromic films in absorbance-modulation-optical-lithography

Apratim Majumder, Phillip L. Helms, Trisha L. Andrew, and Rajesh Menon

Citation: *AIP Advances* **6**, 035210 (2016); doi: 10.1063/1.4944489

View online: <http://dx.doi.org/10.1063/1.4944489>

View Table of Contents: <http://scitation.aip.org/content/aip/journal/adva/6/3?ver=pdfcov>

Published by the *AIP Publishing*

---

### Articles you may be interested in

[Effective medium based optical analysis with finite element method simulations to study photochromic transitions in Ag-TiO<sub>2</sub> nanocomposite films](#)

*J. Appl. Phys.* **119**, 123104 (2016); 10.1063/1.4944806

[Optical properties of TaTe<sub>2</sub>O<sub>7</sub> thin films as absorber materials for extreme ultraviolet lithography binary masks](#)

*J. Vac. Sci. Technol. B* **30**, 06F505 (2012); 10.1116/1.4766879

[Modeling of multilayer electrode performance in transverse electro-optic modulators](#)

*AIP Advances* **1**, 042163 (2011); 10.1063/1.3668284

[Modeling And Analysis Of Lateral Doping Region Translation Variation On Optical Modulator Performance](#)

*AIP Conf. Proc.* **1325**, 297 (2010); 10.1063/1.3537933

[Electron optical performance of electron beam lithography columns predicted by a simple model](#)

*J. Vac. Sci. Technol. B* **7**, 98 (1989); 10.1116/1.584704

---

The cover image for AIP Applied Physics Reviews, featuring a blue and orange color scheme with a molecular structure background. The text 'AIP Applied Physics Reviews' is visible in the top left corner of the cover.

**NEW Special Topic Sections**

**NOW ONLINE**  
Lithium Niobate Properties and Applications:  
Reviews of Emerging Trends

**AIP** Applied Physics Reviews

# A comprehensive simulation model of the performance of photochromic films in absorbance-modulation-optical-lithography

Apratim Majumder,<sup>1</sup> Phillip L. Helms,<sup>1</sup> Trisha L. Andrew,<sup>2</sup>  
and Rajesh Menon<sup>1,a</sup>

<sup>1</sup>*Department of Electrical and Computer Engineering, University of Utah, Salt Lake City, Utah 84112, USA*

<sup>2</sup>*Department of Chemistry, University of Wisconsin-Madison, Madison, Wisconsin 53706, USA*

(Received 18 December 2015; accepted 2 March 2016; published online 14 March 2016)

Optical lithography is the most prevalent method of fabricating micro- and nano-scale structures in the semiconductor industry due to the fact that patterning using photons is fast, accurate and provides high throughput. However, the resolution of this technique is inherently limited by the physical phenomenon of diffraction. Absorbance-Modulation-Optical Lithography (AMOL), a recently developed technique has been successfully demonstrated to be able to circumvent this diffraction limit. AMOL employs a dual-wavelength exposure system in conjunction with spectrally selective reversible photo-transitions in thin films of photochromic molecules to achieve patterning of features with sizes beyond the far-field diffraction limit. We have developed a finite-element-method based full-electromagnetic-wave solution model that simulates the photo-chemical processes that occur within the thin film of the photochromic molecules under illumination by the exposure and confining wavelengths in AMOL. This model allows us to understand how the material characteristics influence the confinement to sub-diffraction dimensions, of the transmitted point spread function (PSF) of the exposure wavelength inside the recording medium. The model reported here provides the most comprehensive analysis of the AMOL process to-date, and the results show that the most important factors that govern the process, are the polarization of the two beams, the ratio of the intensities of the two wavelengths, the relative absorption coefficients and the concentration of the photochromic species, the thickness of the photochromic layer and the quantum yields of the photoreactions at the two wavelengths. The aim of this work is to elucidate the requirements of AMOL in successfully circumventing the far-field diffraction limit. © 2016 Author(s). All article content, except where otherwise noted, is licensed under a Creative Commons Attribution (CC BY) license (<http://creativecommons.org/licenses/by/4.0/>). [<http://dx.doi.org/10.1063/1.4944489>]

## I. INTRODUCTION

In the micro- and nano-patterning industries the traditional methods of fabricating features close to or below the diffraction limit which is classically defined as about a third of the exposure wavelength,<sup>1</sup> are to employ extreme ultraviolet,<sup>2</sup> multiple exposure-and-etch mechanisms<sup>3</sup> or self-aligned patterning techniques.<sup>4</sup> All of these techniques achieve their goal at the cost of increased the processing time, expense and complexity.<sup>5</sup> Recently the diffraction limit has been broken in optical microscopy by techniques like stimulated-emission-depletion (STED) microscopy,<sup>6</sup> photo-activated-localization microscopy (PALM)<sup>7</sup> and stochastic-optical-reconstruction microscopy

---

<sup>a</sup>Email: [rmenon@eng.utah.edu](mailto:rmenon@eng.utah.edu)



(STORM).<sup>8</sup> Primarily inspired by STED, our approach to photolithography, termed absorbance-modulation-optical lithography (AMOL)<sup>9,10</sup> has been experimentally demonstrated<sup>11-13</sup> to possess patterning capabilities beyond the diffraction limit.

Past theoretical studies on AMOL were aimed at analyzing the photochemical processes using a kinetic model of the photochromic reaction.<sup>14</sup> However the role of diffraction of the light upon passage through the AML with complete solutions to Maxwell's equations were ignored. Nevertheless, it was a useful study on the effect of the material parameters on the confinement of the exposing beam PSF. There was also a full-vector finite-element model solved under photostationary conditions to analyze the effect of light polarization on the AMOL process.<sup>15</sup> The paper did not study the effect of changing the material parameters to influence the light absorbance within the AML.

Thus, in order to fully understand the effect of material characteristics in conjunction with the electromagnetic effects within the AML, we have resorted to a full-vector finite-element model that incorporates all the different parameters of interest in AMOL. These include the effects of light polarization and incident illumination patterns, the ratio of intensities of the confining and exposing beams, the thickness of the AML, the concentration of the photochromic species, the photoreaction quantum yields of the two states of the photochromes and their relative absorbances at the two wavelengths. Hence the model described here presents the most comprehensive picture to date, of the lithographic process in AMOL and its governing factors.

## II. MODELING AND SIMULATION

The photochromic compounds used in AMOL that comprise the AML, switch between a form (closed form) that is transparent to an exposure wavelength ( $\lambda_1$ ) and one (open form) that is opaque to it by exposure to a second wavelength ( $\lambda_2$ ), as shown in Fig. 1(a). A lithographic exposure in AMOL is described using the geometry illustrated in Fig. 1(a). Typically the substrate is a silicon wafer on top of which a thin layer of photoresist is spun. The photoresist is the recording medium of the latent image of  $\lambda_1$  (exposing beam). The AML is spun on top of this photoresist layer. Following sample preparation, two standing waves of  $\lambda_1$  and  $\lambda_2$  (confining beam) are incident on the sample such that the peaks of  $\lambda_1$  are collocated with the nodes of  $\lambda_2$ . Under this illumination scheme, the competing action of the two beams converts the AML into the opaque state everywhere except at the node of the  $\lambda_2$  beam and allows spatially confined photons of  $\lambda_1$  to penetrate through this aperture and expose the photoresist layer. This two-dimensional geometry is consistent with our experiments.<sup>13</sup> In order to model and solve the photochemical reactions and the light-material interactions in this geometry, the finite-element method (FEM) (provided by commercial FEM software COMSOL, interfaced with MATLAB) was chosen due to its ability to effectively handle dispersive media and material-based inhomogeneities, and solve Maxwell's equations based on user defined material properties.

In modelling the photochemical reactions that occur within the AML, the following general hypotheses<sup>11</sup> are considered that have been separately verified in the past by experiments. The

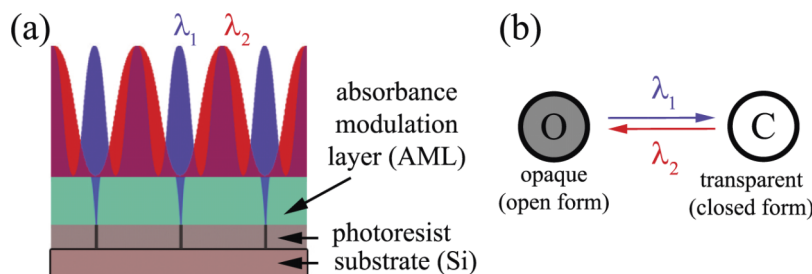


FIG. 1. (a) Schematic of AMOL showing simultaneous illumination of the AML by standing waves of  $\lambda_2$  at 647 nm and  $\lambda_1$  at 325 nm to render the AML opaque to only the regions under the  $\lambda_2$  peaks. This system in conjunction with the photochemical interconversion of the two species shown above allows the photoresist to be exposed by only  $\lambda_1$  photons that are restricted to dimensions below the diffraction limit. (b) UV-Vis spectrophotometry data showing the absorbance of the two forms (open and closed) at different wavelengths.

conversion from the open form of the photochrome (denoted by O) to the closed form (denoted by C) and the reverse reaction are only light driven upon the absorbance of wavelengths  $\lambda_1$  and  $\lambda_2$  respectively. Both states exhibit thermal stability as verified by previous experiments.<sup>11–13</sup> The absorbance data for these photochromes is shown in Ref. 16. In general, this conversion reaction follows first-order kinetics and the conversion rate of either species within the AML is dependent on the instantaneous molar concentration of the species (denoted [O] or [C]), the intensity of the wavelength ( $I_1$  for  $\lambda_1$  and  $I_2$  for  $\lambda_2$ ), the molar absorptivity at the specific wavelengths ( $\varepsilon_{ij}$ , e.g. denoted by  $\varepsilon_{1O}$  for open form at  $\lambda_1$ ) and the quantum yield of the photochemical reactions ( $\varphi_{ij}$ , e.g. denoted by  $\varphi_{OC}$  for conversion from open to closed form). Thus, assuming the two states are in dynamic equilibrium and following the approach adopted in previous work,<sup>11,17</sup> the rate equation for the photo-transition reaction is expressed as  $-\frac{\partial[O]}{\partial t} = [O]I_1\varepsilon_{1O}\varphi_{OC} - [C]I_2\varepsilon_{2C}\varphi_{CO} - [C]I_1\varepsilon_{1C}\varphi_{CO}$ . From the conservation of mass, we have  $[O] + [C] = [O]_0$ , where  $[O]_0$  is the initial concentration under the assumption that the initial state is composed only of the open form. Solving this equation for the photostationary state where  $\frac{\partial[O]}{\partial t} = 0$ , the following expressions can be derived:

$$\frac{[C]}{[O]_0} = x_C = \frac{1}{1 + I_2/I_1\varepsilon_{2C}/\varepsilon_{1O}\varphi_{CO}/\varphi_{OC} + \varepsilon_{1C}/\varepsilon_{1O}\varphi_{CO}/\varphi_{OC}} \quad (1)$$

where  $x_C$  is the mole fraction for the closed form. The mole fraction of the open form is thus  $x_O = (1 - x_C)$ . It can be clearly seen that the material parameters that influence how much of the two photochromic species undergo conversion are not only the intensity ratio ( $I_2/I_1$ ), but also the ratio of the molar absorptivity ( $\varepsilon_{2C}/\varepsilon_{1O}$  and  $\varepsilon_{1C}/\varepsilon_{1O}$ ) and the ratio of the quantum yields of the photochemical reactions ( $\varphi_{CO}/\varphi_{OC}$ ). The overall absorbance ( $\alpha_{\lambda i}$ ) at each wavelength can now be derived from the absorbance of the individual species ( $\alpha_{\lambda iO}$  and  $\alpha_{\lambda iC}$ ) as  $\alpha_1 = \alpha_{1O}x_O + \alpha_{1C}x_C$  and  $\alpha_2 = \alpha_{2O}x_O + \alpha_{2C}x_C$ . This translates to the imaginary part of the refractive index for the AML for  $\lambda_1$  as  $k_1 = \alpha_1\lambda_1/4\pi$  and for  $\lambda_2$  as  $k_2 = \alpha_2\lambda_2/4\pi$ . Additionally, the intensity of light for either wavelength inside the photochromic layer is given by Beer Lambert's law of the general form  $\log \frac{I_1}{I_1} = \varepsilon cl$ , where  $c$  and  $l$  are concentration and depth respectively. The different parameters corresponding to the AML are presented in Ref. 16.

### III. RESULTS

A representative solution of the model constructed in COMSOL is shown in Fig. 2(a) with 100 nm thick AML and 60 nm thick photoresist and an intensity ratio of 2000. The full vector solutions of Maxwell's equations inside the AML reveals the exact light pattern, while the AMOL governing equations show the distribution of the photochromic species inside the depth of the AML. This knowledge cannot be acquired by scalar modelling considering only the intensity distribution on the top of the AML.<sup>14</sup> In order to explore the effect of light polarization and the incident illumination pattern on AMOL aperture formation, the polarization for  $\lambda_1$  is varied between TE and TM. For  $\lambda_2$  the polarization is kept fixed as TE for the highest contrast standing wave formation. The period for the  $\lambda_2$  standing wave is taken as 325 nm, consistent with previous experiments.<sup>11</sup>

For  $\lambda_1$ , four types of spatial patterns are considered to demonstrate the effect of spatial arrangement of the two beams in AMOL: uniform illumination, standing waves with periods twice, equal to and half that of the  $\lambda_2$  standing wave. Figs. 2(b) and 2(c) show the confinement achieved for the  $\lambda_1$  PSF for these different illumination schemes and for different  $\lambda_1$  polarizations. Exact variations of the  $\lambda_1$  PSF with the intensity ratio for both polarizations is shown in Ref. 16. Good confinement can only be achieved with TM polarized writing beam, consistent with what has been previously reported.<sup>15</sup> Varying the period of  $\lambda_1$  does not affect the final Full-width-half-maximum (FWHM) for either polarization to a great extent for TM polarization. The model shows that the system is able to resolve isolated features down to  $\sim 20$  nm separated by the period of  $\lambda_2$  standing wave. However multiple exposures can increase pattern resolution. A detailed discussion is presented in Ref. 16.

Although Fig. 2 indicates that the final FWHM value of the transmitted PSF of the exposing beam ( $\lambda_1$ ) is independent of the spatial pattern of the incident beams, the FEM model reveals that for  $\lambda_1$  period being half that of  $\lambda_2$ , suppressed peaks are formed (Fig. 3(a)) wherever peaks of both

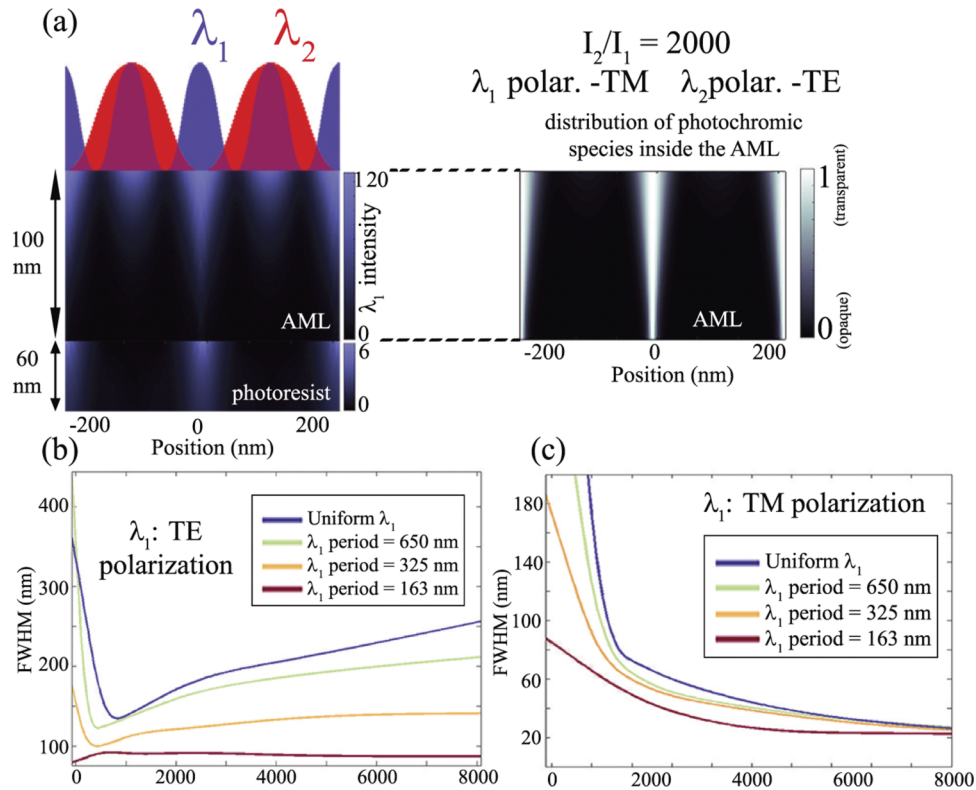


FIG. 2. (a) Results of the FEM model showing the  $\lambda_1$  intensity and corresponding distribution of the photochromic species inside the AML for an intensity ratio of 2000 and TM polarized  $\lambda_1$ . (b)-(c) FWHM of transmitted PSFs of the  $\lambda_1$  v/s different intensity ratios for TE and TM polarizations.

beams coincide. This was previously observed experimentally<sup>11</sup> and this is the first time it is being demonstrated with theoretical modelling. Three-dimensional PSFs that are of importance when patterning aperiodic two dimensional structures are provided in Ref. 16.

Uniform illumination seems to provide the sharpest PSF at the loss of some contrast (Fig. 3(d)). Hence it can be seen that the most important factor that governs the lithographic process in AMOL and allows for sub-diffraction confinement of the exposing beam is the ratio of the intensities i.e.  $I_2/I_1$ , predicting a FWHM linewidth of about 20-30 nm for an intensity ratio of about 6000. This is the most critical governing factor in AMOL and is similar to the scaling trend in STED microscopy. Unlike conventional photolithography, where the feature sizes scale with absolute intensity of the exposing beam, in AMOL the scaling occurs with respect to the intensity ratio. This introduces the nonlinearity effect required to successfully carry out double exposures without in between etch steps.

Since the absorption of  $\lambda_1$ , ideally at all locations other than the exact vicinity of the optical node at  $\lambda_2$  is critical to improving the contrast of the lithographic procedure, clearly the concentration of the open form and hence the film thickness of the AML is expected to play an important role. A plot of the thickness of the AML versus the FWHM of the transmitted dose, for two intensity ratios 1000 and 4000 is shown in Fig. 4(a). Contrary to previous work using scalar theory<sup>14</sup> the FEM results reveal that the PSF FWHM does not monotonically decrease with increasing thickness but instead decreases till a certain thickness value before increasing again. The reason for this may be due to the fact that past a certain thickness even though the aperture in the AML shrinks to a FWHM of a few nanometers, there is not enough difference in the imaginary part of the refractive index between the open and closed forms for the light to shrink down further as shown in Fig. 4(c). Past this point the light behaves as if simply propagating through an effective medium and actually spreads out with an accompanied loss in contrast. Exact PSF scaling as shown in Ref. 16 also shows that the suppressed peaks are also observed to become more prominent. Figures 4(b) shows the

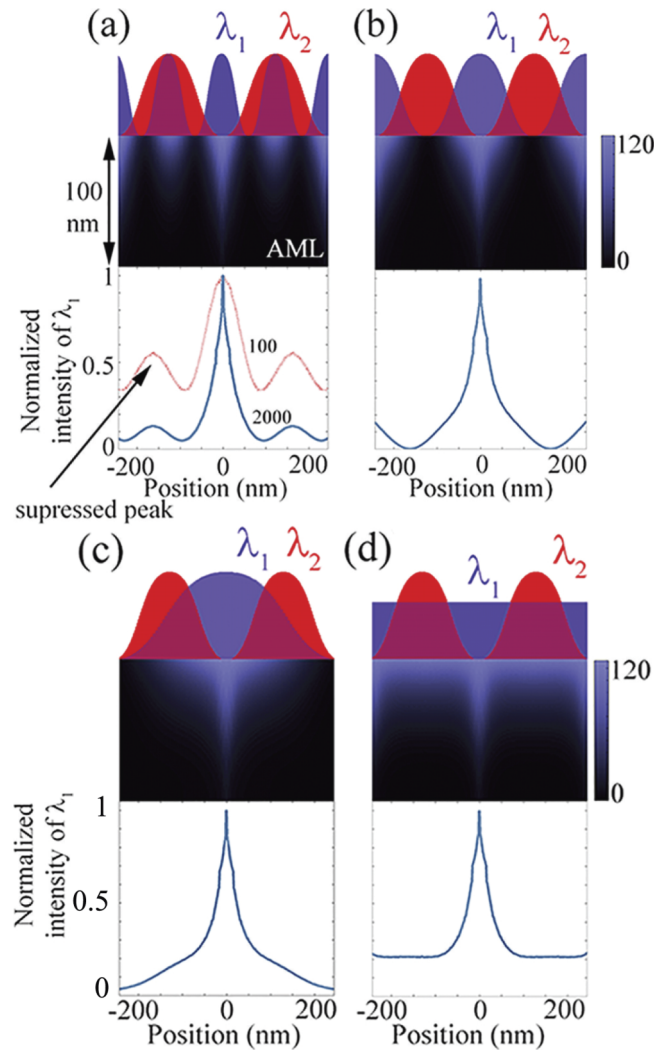


FIG. 3. (a)-(d) FEM solutions for different illumination schemes where the period  $\lambda_1$  standing wave is varied. Suppressed peaks form where the peaks of both beams coincide. Contrast loss occurs for uniform  $\lambda_1$  illumination.

effect of increasing the concentration of the photochromes in the AML. Increased concentration can achieve narrow PSFs at much lower AML thickness and intensity ratios. This work is currently being pursued using evaporated thin films of the photochromes<sup>18</sup> and photochromic polymers.

The third factor of interest are the two quantum yields of the photoreaction - from the open to the closed form and vice versa, i.e.  $\varphi_{OC}$  and  $\varphi_{CO}$ . It is indicated that good confinement can be achieved with intensity ratio as small as 10 provided that  $\varphi_{CO}/\varphi_{OC}$  is high, as presented in Fig. 5(a), for a fixed AML thickness of 100 nm. Exact PSF behavior as shown in Ref. 16. However so far only the photochrome 1,2-bis(5,5'-dimethyl-2,2'-bithiophen-4-yl)perfluorocyclopent-1-ene (otherwise referred to as BTE) of the diarylethene family has been used in successful experiments and for that the  $\varphi_{CO}$  of  $8.8 \times 10^{-4}$  is several orders of magnitude lower than the  $\varphi_{OC}$  of 0.24. Synthesis of other diarylethene based molecules with more closely matched quantum yields in the future can yield better results in AMOL. Interestingly, at higher intensity ratios with higher values of  $\varphi_{CO}/\varphi_{OC}$ , the FWHM actually first decreases sharply and then increases since the aperture inside the AML approaches a negligible width and this appears simply as an effective medium to  $\lambda_1$  photons, as shown in Fig. 5(b) where the distribution of the photochromes inside the AML are compared for intensity ratios of 10 and 100 and  $\varphi_{CO}/\varphi_{OC}$  values of BTE and a hypothetical value of 0.2.

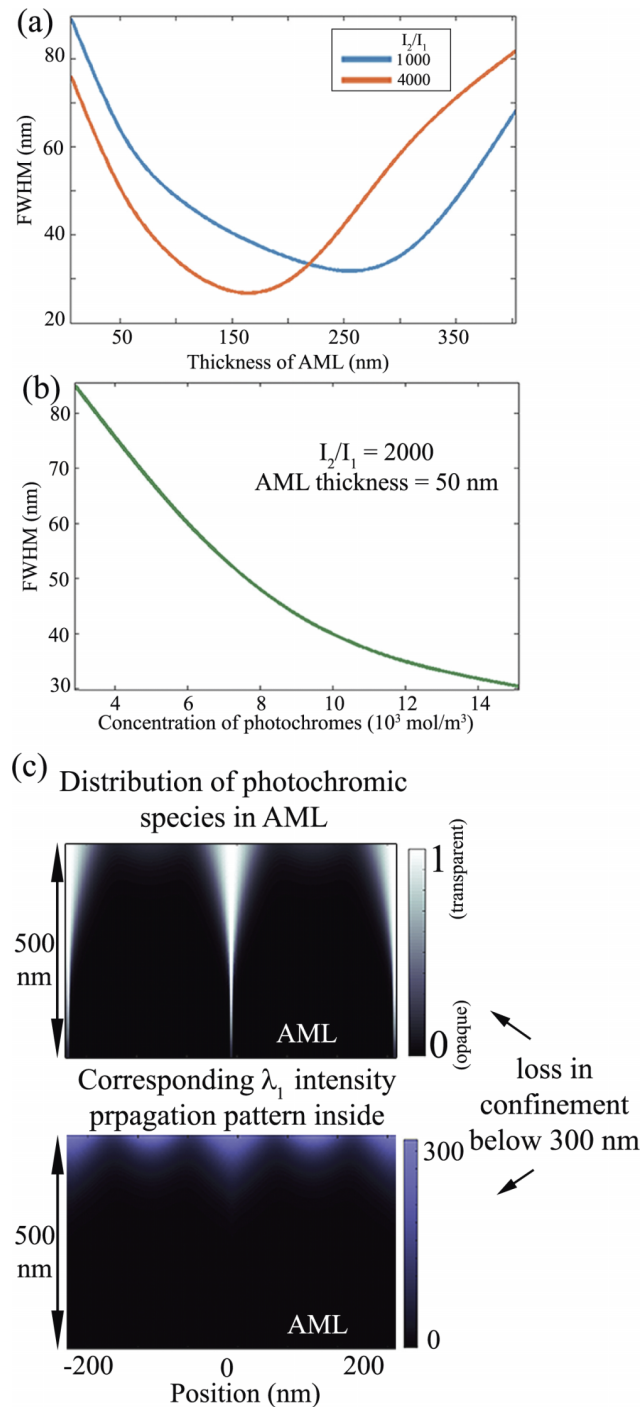


FIG. 4. (a) FWHM of  $\lambda_1$  PSF v/s AML thickness. Contrary to previous work<sup>14</sup> FWHM does not monotonically decrease with increased AML thickness, rather reaches a minimum and then increases. (b) FWHM of  $\lambda_1$  PSF v/s concentration of photochromes for an intensity ratio of 2000 and AML thickness of 50 nm. (c) FEM solutions showing the depth profile inside the AML for the AMOL aperture and corresponding exposing beam intensity. Loss of light confinement occurs at depths greater than 300 nm where the opacity difference becomes negligible.

The last parameter of interest, the molar absorptivity at the exposing wavelength shows the same trend as that seen in the case of quantum yield, contrary to previous work.<sup>14</sup> Basically increasing  $\epsilon_{1C}/\epsilon_{1O}$  (the ratio of absorbances of the two species at the exposing beam) at first improves the contrast before the aperture inside the AML becomes negligible small for the light to guide through.

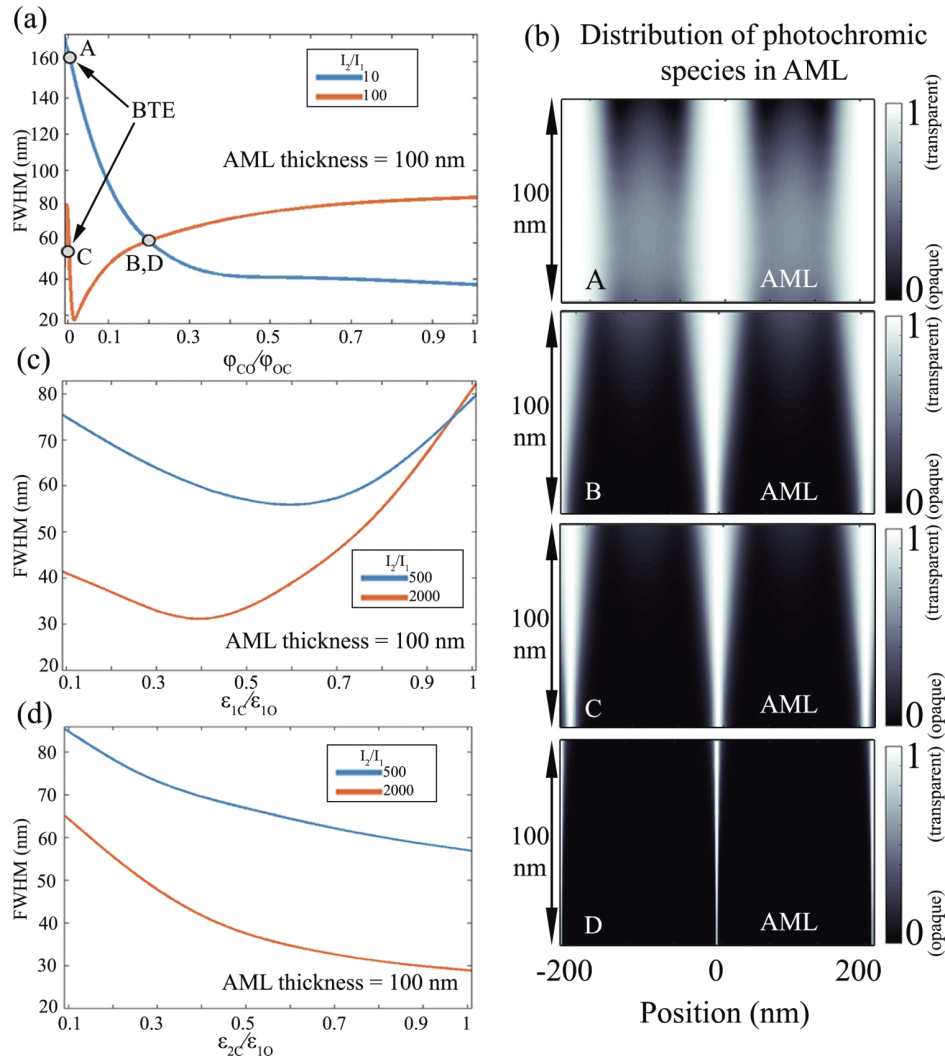


FIG. 5. (a) FWHM of  $\lambda_1$  PSF v/s ratio of quantum yields. Contrary to previous work<sup>14</sup> FWHM does not monotonically decrease with increased quantum yield ratio for higher intensity ratios, rather reaches a minimum and then increases. (b) FEM solutions showing the depth profile inside the AML for the AMOL aperture and corresponding exposing beam intensity. (c) FWHM of  $\lambda_1$  PSF v/s  $\epsilon_{1C}/\epsilon_{1O}$ . (d) FWHM of  $\lambda_1$  PSF v/s  $\epsilon_{2C}/\epsilon_{1O}$ .

However the FWHM appears to monotonically decrease with increasing  $\epsilon_{2C}/\epsilon_{1O}$  though the effect is far less pronounced since as equation (1) shows, the effect of this parameter is largely scaled by the intensity ratio, the value of which has a more profound influence on the AMOL process.

#### IV. CONCLUSION

This is most comprehensive and explanatory modelling of the AMOL process that clearly demonstrates the effect of the various parameters on the process. Increasing the intensity ratio of the two beams allows for greater confinement of the PSF but the effect can also be achieved at lower intensity ratios using photochromic material better suited to the process. The aim is to synthesize such materials with better matched quantum yields for the photokinetics.

#### ACKNOWLEDGEMENT

We would like to thank Benjamin J. Pollock at the University of Wisconsin-Madison and Farhana Masid and Precious Cantu at the University of Utah for helpful insight to the AML.

Financial support from NSF, DARPA and the Utah Science, Technology and Research (USTAR) initiative are also gratefully acknowledged.

- <sup>1</sup> E. Abbé, *Arch. Mikrosk. Anat. Entwicklungsmech* **9**(1), 413–418 (1873).
- <sup>2</sup> O. Wood *et al.*, *Proc. SPIE* **7271**, 727104 (2009).
- <sup>3</sup> B. Haran *et al.*, Electron Devices Meeting (IEDM), 2008 IEEE International, 1-4 (2008).
- <sup>4</sup> S. Natarajan *et al.*, Electron Devices Meeting (IEDM), 2014 IEEE International, 3.7.1-3.7.3 (2014).
- <sup>5</sup> P. Zimmerman, *SPIE Newsroom*, 10.1117/2.1200906.1691, 1-3 (2009).
- <sup>6</sup> S. W. Hell and J. Wichmann, *Opt. Lett.* **19**(11), 780–782 (1994).
- <sup>7</sup> E. Betzig, J. K. Trautman, T. D. Harris, J. S. Weiner, and R. L. Kostelak, *Science* **251**(5000), 1468–1470 (1991).
- <sup>8</sup> M. Rust, M. Bates, and X. Zhuang, *Nature Methods* **3**(10), 793–796 (2003).
- <sup>9</sup> R. Menon and H. I. Smith, *J. Opt. Soc. Am. A* **23**(9), 2290-2294 (2006).
- <sup>10</sup> R. Menon, Hsin-Yu Tsai, and S. W. Thomas III, *Phys. Rev. Lett.* **98**(4), 043905-1-4 (2007).
- <sup>11</sup> T. L. Andrew, H.-Y. Tsai, and R. Menon, *Science* **324**, 917-921 (2009).
- <sup>12</sup> F. Masid, T. L. Andrew, and R. Menon, *Opt. Exp.* **21**(4), 5209-5214 (2013).
- <sup>13</sup> A. Majumder, F. Masid, B. J. Pollock, T. L. Andrew, and R. Menon, *Opt. Exp.* **23**(9), 12244-12250 (2015).
- <sup>14</sup> G. Pariani, R. Castagna, R. Menon, C. Bertarelli, and A. Bianco, *Opt. Lett.* **38**(16), 3024-3027 (2013).
- <sup>15</sup> J. E. Foulkes and R. J. Blaikie, *J. Vac. Sci. Tech. B* **27**, 2941-2946 (2009).
- <sup>16</sup> See supplementary material at <http://dx.doi.org/10.1063/1.4944489> for detailed analyses of photochromic behavior.
- <sup>17</sup> M. Warner and R. J. Blaikie, *Phys. Rev. A* **80**(3), 03833 (2009).
- <sup>18</sup> P. Cantu, T. L. Andrew, and R. Menon, *App. Phys. Lett.* **105**, 193105 (2014).